Chemical Engineering Journal 396 (2020) 125312

Contents lists available at ScienceDirect

Chemical Engineering Journal

journal homepage: www.elsevier.com/locate/cej

A novel ternary mica-titania@rGO composite pearlescent pigment for the photocatalytic degradation of gaseous acetaldehyde

Xiangming Fang[a,b], Guanhong Lu[b], Asad Mahmood[b], Yan Wang[b,*], Xiao Wang[b], Xiaofeng Xie[b], Zhihong Tang[a], Jing Sun[b]

[a] University of Shanghai for Science and Technology, 516 Jungong Road, Shanghai 200093, China
[b] State Key Laboratory of High Performance Ceramics and Superfine Microstructure, Shanghai Institute of Ceramics Chinese Academy of Sciences, 1295 Dingxi Road, Shanghai 200050, China

HIGHLIGHTS

- A novel ternary pearlescent composite is fabricated to photodegrade VOCs.
- MT@rGO-0.1 composite shows enhanced photocatalytic activity and stability.
- Superoxide radicals ($\cdot O_2^-$) play a major role in the photodegradation.
- The composite is expected to apply as car paint additive to purify air.

GRAPHIC ABSTRACT

The novel MT@rGO composite has significantly enhanced photocatalytic degradation performance and unique silver sparkling luster effect.

The MT@rGO pearlescent pigment composite is expected to coat on the surface of automobile to purify air.

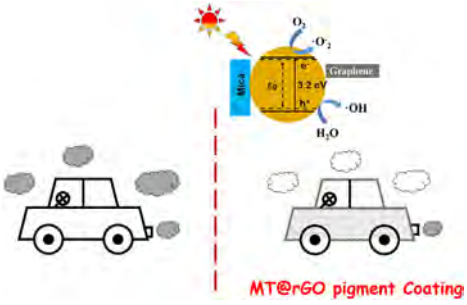

ARTICLE INFO

Keywords:
Mica
Graphene
Photocatalytic degradation
Flowing gaseous acetaldehyde
Pearlescent pigment

ABSTRACT

The photocatalytic application of TiO_2 is limited due to low light harvesting abilities in the whole solar spectrum and fast recombination of the photoinduced electron-hole pairs. Herein, we report a TiO_2-based ternary composite photocatalyst (MT@rGO-x; x = 0.05–0.2) with a pearlescent color effect, which incorporates a mica reflection core and a rGO multifunctional shell as cocatalysts. The micro flake composites were synthesized by a facile precipitation route and applied first to photodegrade gaseous acetaldehyde. MT@rGO-0.1 composite has optimal performance, which is 2.5 times photodegradation efficiency and 3 times CO_2 mineralization efficiency higher than those of pure TiO_2. The enhanced photocatalytic performance of MT@rGO composite is associated with effectively improved light harvesting of TiO_2 by mica reflection. The presence of rGO facilitates the separation of electron-hole pairs and pollutant absorption. In addition, the superoxide radical was proved as the decisive active species for the photodegradation of acetaldehyde by electron spin resonance analyses and radical quenching tests. Our MT@rGO photocatalyst is expected to be applied as a functional and decorative additive of car paint, which is subject to photodegradation due to air pollutants.

* Corresponding author.
E-mail address: wangyan@mail.sic.ac.cn (Y. Wang).

https://doi.org/10.1016/j.cej.2020.125312
Received 9 December 2019; Received in revised form 9 April 2020; Accepted 1 May 2020
Available online 06 May 2020
1385-8947/ © 2020 Elsevier B.V. All rights reserved.

1. Introduction

Low boiling point volatile organic compounds (VOCs), such as acetaldehyde in indoor and outdoor air, contribute to atmospheric pollution and cause serious health problems in humans [1-4]. To solve this problem, several air purification techniques have been proposed [5,6]. The photodegradation of VOCs is considered as a promising solution, which utilizes light harvesting in the solar spectrum by a photocatalyst [7,8]. One of the most researched semiconductor photocatalysts, anatase TiO_2, is preferred owing to its abundance, nontoxicity, and stability [9,10]. However, anatase TiO_2 with a wide bandgap of 3.2 eV suffers from limited light harvesting and fast recombination of photogenerated electron-hole pairs [11,12]. Therefore, many attempts have been reported to overcome these shortcomings, including doping [13,14], modification of surface chemical states by depositing cocatalysts [15], formation of heterojunctions by semiconductors hybridizing [16], and morphology manipulations [17].

Recently, reduced graphene oxide (rGO) with a large surface area, excellent optical properties and high conductivity has been widely studied to enhance the photocatalytic performance of TiO_2 [18,19]. For instance, Yue et al. deposited TiO_2 onto the surface of graphene to form a 2D–2D microporous structure composite. The degradation efficiency of toluene increased by a factor of 1.4, which was attributed to the improvement of the adsorption capacity and separation efficiency [20]. In our previous work, a rGO-TiO_2 binary nanocomposite was fabricated to enhance the degradation of gaseous acetaldehyde and o-xylene by increasing adsorption of VOCs and prolonging the charge carrier lifetime of TiO_2 [21]. Furthermore, beyond binary composites, ternary rGO-TiO_2 hybrid composites are expected to provide insight into novel 3D nanoarchitectures with enhanced photocatalytic properties [22,23]. Zhang et al. fabricated the ternary hybrids of CdS/rGO/TiO_2 to selectively oxidize alcohols to corresponding aldehydes with enhanced visible light harvesting [24]. Wu et al. prepared g-C_3N_4/rGO/TiO_2 ternary heterojunctions with four times higher photodegradation of methylene blue under simulated solar light irradiation, which was ascribed to the promoted separation and transfer of charge carriers [25]. In brief, the enhanced photocatalytic activity of rGO-based photocatalysts is associated with longer lifetime of the photogenerated electron-hole pairs, a faster rate of charge transfer, and improved pollutant capture [26,27].

The photocatalytic performance of composites could also benefit from increased light harvesting by introducing a reflection center. However, this has not received much attention. Mica with a stoichiometric formula $KAl_2(AlSi_3O_{10})(OH)_2$ has high reflectivity and is widely applied as a paint additive [28,29]. Moreover, with increasing thickness, mica has a wide bandgap from 2.5 eV to 7.85 eV [30]. Thus, mica could be expected to serve as a reflection center and cocatalyst.

Given the relationship between the structure fabrication and photocatalytic activity of a photocatalyst, we propose a novel tripartite-structure mica-titania@reduced graphene oxide (MT@rGO) composite for the degradation of flowing gaseous acetaldehyde. Mica serves as a reflection center to increase the light harvesting of TiO_2 nanoparticles (NPs). The wrapped rGO outer layer is used to adsorb more pollutants and facilitate electron-hole pair separation. The structure-active relationship of MT@rGO composite is confirmed by the increased acetaldehyde photodegradation efficiency and CO_2 mineralization activity. Moreover, the high performance of MT@rGO composite with a pearlescent effect is anticipated to find application in car paint as a functional and decorative additive.

2. Experimental

2.1. Materials and reagents

Mica was supplied by Hangzhou Forward Fine Chemicals Co., Ltd., China, and its particle size distribution ranged from 10 to 60 μm. Acetaldehyde gas (1000 ppm) was purchased from Shanghai Weichuang Standard Gas Analytical Technology Co., Ltd. Graphite flakes were bought from Alfa Aesar (325 mesh). Zinc powder (D50 < 50 μm) was obtained from Aladdin Reagent Co., Ltd., and 5,5-dimethyl-1-pyrroline N-oxide (> 99%) was purchased from DOJINDO Laboratories. All other chemicals and solvents were purchased from Shanghai Sinopharm Chemical Reagent Co., Ltd. (Shanghai, China) and used without further purification.

2.2. Synthesis

The mica-titania@reduced graphene oxide (MT@rGO) composites were synthesized according to our previous work with some modifications [31]. First, 2 M $TiCl_4$ aqueous solution was hydrolyzed on the surface of mica flakes to synthesize MT. For comparison, as-prepared TiO_2 nanoparticles were synthesized by the same procedure without mica. Second, MT powder and GO nanosheets were separately dispersed in HCl solution (pH = 4). The different volumes of GO solution were dropwise added into the MT suspension to obtain MT@GO composites under stirring. The samples were denoted with different added amounts of GO in MT@GO composites as MT@GO-x (0.05–0.2 wt%). Finally, 50 mg of zinc powder was used to reduce the 1.0 g MT@GO composite in 10 mL of HCl solution (35 wt%). The excess HCl ensured complete dissolution of the zinc. The as-prepared MT@rGO-x (x = 0.05–0.2 wt%) composites were obtained after filtration, washing and drying.

2.3. Characterization

X-ray diffraction (XRD, BRUKER AXS GmbH, Germany) with Cu Ka radiation of wavelength λ = 0.154 nm was used for the crystalline phase analysis. A field emission scanning electron microscope (Magellan 400 FEI) with an operating voltage of 10 kV was employed to investigate the surface and cross-sectional morphology of the composites. The electric resistivity was measured on a semiconductor volume resistivity measuring instrument (ST2722, Suzhou Jingge Electronic Co. LTD) at 9.8 MPa. Raman spectra were collected by a DXR Raman Microscope (Thermo Fisher Scientific) using a laser with an excitation wavelength of 532 nm at 7 mW of laser power. X-ray photoelectron spectroscopy (XPS) analysis was conducted using a twin anode gun, Mg Ka (1253.6 eV) (Microlab 310F Scanning Auger Microprobe, VG Scientific Ltd). A Perkin–Elmer Lambda 950 spectrometer with an integrating sphere was applied to record the UV–vis diffuse reflectance spectroscopy and colorimetric values of the Commission Internationale de l'Eclairage (CIE) 1976 L*a*b* of the synthesized powder. The photocurrent response and electrochemical impedance spectroscopy of the as-prepared samples were evaluated using a CHI660D electrochemical workstation in a conventional three-electrode quartz cell. The photoluminescence spectra (PL, Hitachi F-4600) were acquired with an excited wavelength of 280 nm. The Brunauer–Emmett–Teller specific surface area (S_{BET}) of the sample was analyzed by a Micromeritics ASAP 3000 nitrogen adsorption apparatus. All samples were degassed at 120 °C for 24 h prior to nitrogen adsorption measurements. The electron spin resonance (ESR) signal of active radicals trapped by DMPO was recorded on a JES-FA200 spectrometer.

2.4. Photocatalytic experiments

The photodegradation of acetaldehyde was carried out in a real-time gas chromatograph monitoring system (Fig. 1). A 120 mL cuboid quartz vessel as a reaction chamber was coupled with a 400 W xenon lamp (CEL-WLAX500, Beijing Zhongjiao Jinyuan Technology Co., Ltd). The concentration of acetaldehyde was monitored by gas chromatography (GC-7920) at 5 min intervals. The experimental process is shown as follows: 0.1 g of sample was dispersed in 2 mL of ethanol solution and uniformly drop-casted on a 15 cm (L) × 7.5 cm (W) × 3

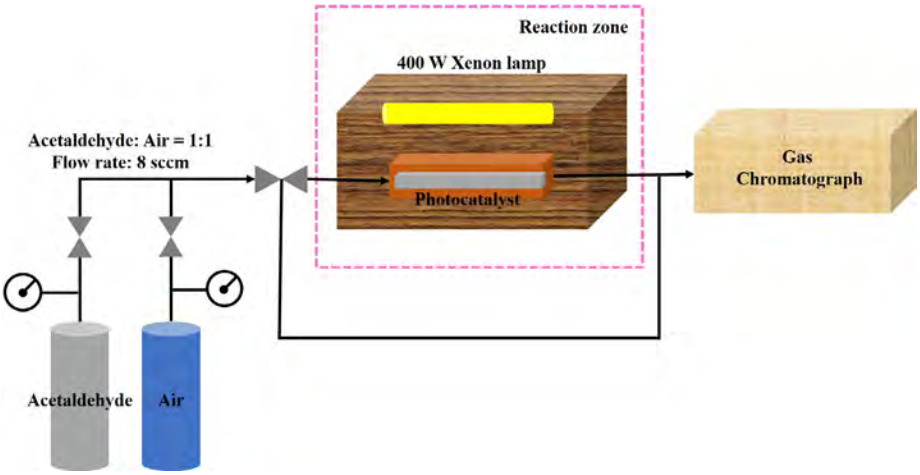

Fig. 1. Real-time gas chromatograph monitoring system.

(H) mm glass plate. After drying, the glass plate was sealed in the vessel. With an 8 sccm flowrate of 500 ppm acetaldehyde, the adsorption–desorption equilibrium of the sample was obtained and then xenon lamp irradiated. The removal rate (η) of acetaldehyde was calculated as$\eta = \left(1 - \frac{C}{C_0}\right) \times 100\%$, where C_0 is the initial concentration and C is the time-dependent concentration of acetaldehyde after irradiation. The cyclic experiment was carried out under the same procedure, and the time interval between two cycles was 3 days.

3. Results and discussion

3.1. Phase structure and morphology

The phase structures of as-prepared TiO_2 NPs, mica, MT and MT@rGO-x (x = 0.05–0.2) composites were studied by XRD as shown in Fig. 2. The XRD peaks at 2θ = 25.60° correspond to the (1 0 1) plane of anatase TiO_2 (JCPDS no. 21–1272). The four sharp peaks of MT appearing at 17.62, 26.52, 35.08, and 45.43° are attributed to the peaks of muscovite (JCPDS no. 76–929), which is similar MT@rGO-x (x = 0.05–0.2) composites. Thus, anatase TiO_2 and mica stably existed in the ternary composite during the preparation process without phase transformation. Nevertheless, the absence of typical rGO peaks at 2θ angles of 10.9° and 24.57° was caused by its low amount, which was less than the limit detection of XRD (ca. 3 wt%) [32,33]. Most importantly, the mass percentage of anatase TiO_2 in MT was approximately 16.9 wt% calculated by Rietveld refinement of XRD data.

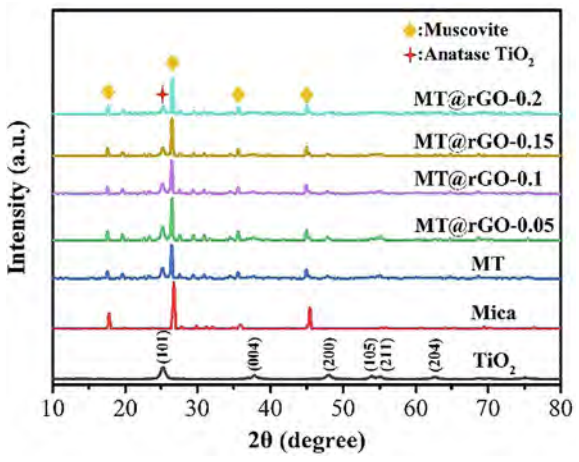

Fig. 2. XRD patterns of as-prepared TiO_2 NPs, mica, MT and MT@rGO-x (x = 0.05–0.2) composites.

The surface and cross-sectional morphologies of as-prepared TiO_2 NPs, MT and MT@rGO-0.1 composite were characterized by FESEM as shown in Fig. 3. The surface micrographs of TiO_2 and MT revealed a small particle size (approximately 10–20 nm) distribution of TiO_2 NPs (Fig. 3a and b). The shapes of MT and MT@rGO-0.1 composite were flat and irregular flakes, whose particle diameter size ranged from 10 to 60 μm (Fig. 3c and d). rGO sheets with wavy wrinkles coated the surface of MT (Fig. 3d-f), as indicated by the yellow arrows.

Generally, the optical thickness of a material is directly related to its geometrical thickness and refractive index by the following equation: $\delta_t = n\delta$, where δ_t, n, and δ are the optical thickness, refractive index, and geometrical thickness, respectively. As presented in Fig. 3g, the thickness of inner mica is approximately 250 nm, and the outer layer of TiO_2-rGO with a comparatively uniform thickness distribution is 43.5 ± 8 nm. Thus, the optical thickness of TiO_2 is approximately 111 nm ± 20 nm with n_{TiO2} = 2.55, which suggests that MT@rGO-0.1 composite could show a silver pearlescent effect [34]. MT@rGO-0.1 composite can be effectively characterized without conductive treatment compared to MT, which indicates MT@rGO-0.1 with enhanced conductive performance after reduction. The volume resistivity (V_R) of the ternary composites was measured at a pressure of 9.8 MPa. The V_R values of MT@rGO-x (x = 0.05–0.2) composites were 3–9 times lower than that of MT (Table S1). Thus, rGO can improve the conductivity of ternary composites, which may ultimately affect their photocatalytic activity.

EDS element mapping profiles were collected to characterize the elemental distributions of MT@rGO-0.1 composites. The white part in Fig. 4a, indicated by the yellow circle, corresponds to the graphene nanosheets. The elemental profile of carbon confirms the uniformly and partial rGO covering on the surface of MT (Fig. 4b).

Raman spectra were used to characterize the local order characteristics of TiO_2 and the structural changes of graphene nanosheets before and after reduction [35-37]. The characteristic Raman modes of TiO_2 were observed around 144, 397, 517, and 638 cm^{-1} which corresponded to $E_{g(1)}$, $B_{1g(1)}$, A_{1g} + $B_{1g(2)}$, and $E_{g(2)}$ (Fig. 5a) [38]. These results suggest that anatase TiO_2 existed in the ternary composites, which is consistent with the XRD result. The typical bands of MT@rGO-0.1 composite at 1338 cm^{-1} and 1594 cm^{-1} are assigned to the D band (lattice disorders at the edges and surfaces of small sp^2 clusters) and G band (first-order scattering of the E_{2g} phonons) (Fig. 5b). The intensity ratio (I_D/I_G) increased from 0.97 (MT@GO-0.1) to 1.70 (MT@rGO-0.1), proving that rGO was successfully obtained [39].

XPS was performed to systematically analyze the surface chemical states and interactions of MT and rGO before and after reduction. The full-range survey XPS of MT@GO-0.1 and MT@rGO-0.1 composites are shown in Fig. 6a. The result reveals Ti, O, and C elements, whose

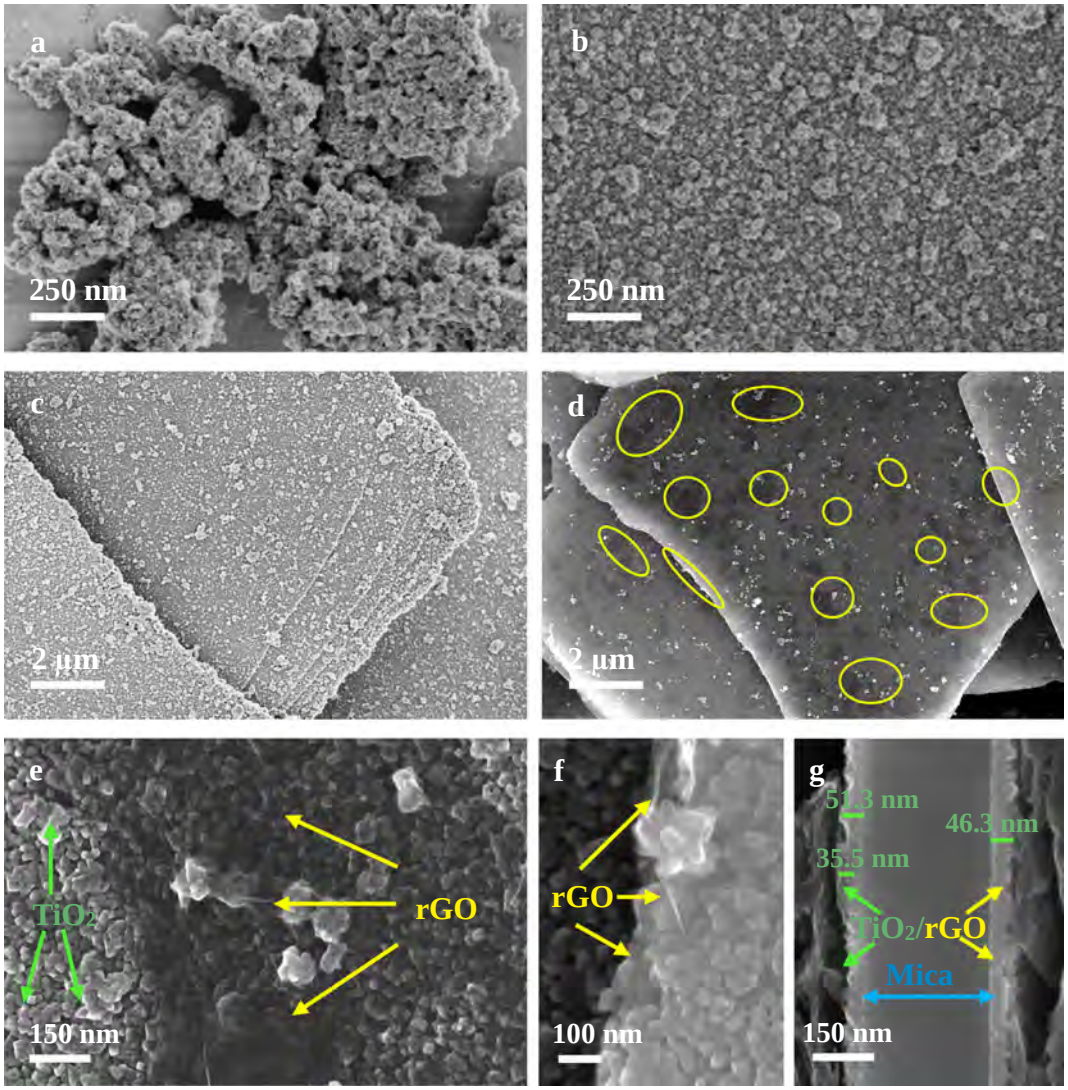

Fig. 3. Surface SEM images of the as-prepared (a) TiO_2 NPs, (b and c) MT, (d-f) MT@rGO-0.1 composite; (g) cross-sectional SEM image of MT@rGO-0.1 composite.

chemical binding energies are Ti2p (456.3 eV), O1s (527.6 eV), and C1s (285.0 eV), respectively. The peak centered at 285.0 eV is assigned to the graphene sp^2 hybridized carbon (C–C) [40]. The peaks at higher binding energies are attributed to oxygen-containing species, which include C–O (286.5 eV) and C=O (289.4 eV). In contrast to the C1s spectrum of MT@GO-0.1 composite, the intensity of C-O and C=O peaks in MT@rGO-0.1 composite significantly decreased (Fig. 6b-c), which confirmed the efficient removal of oxygen-containing functional

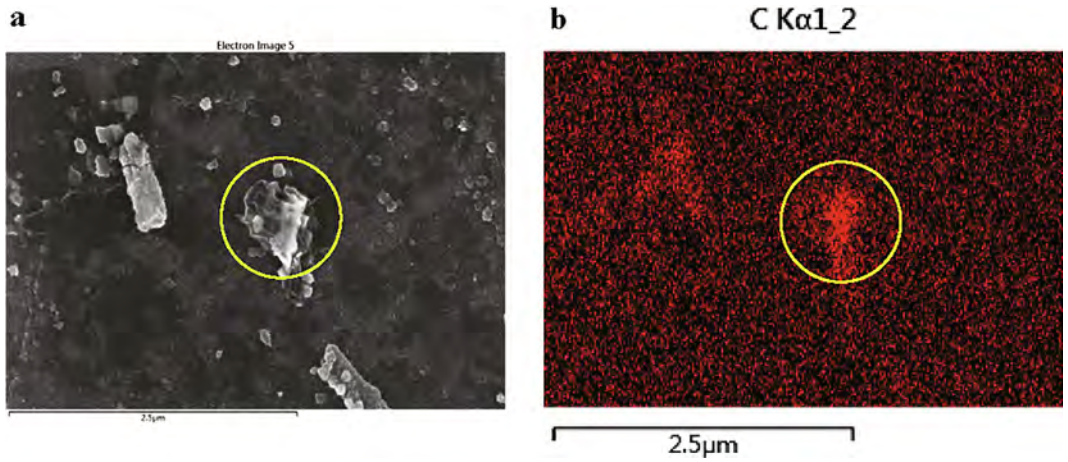

Fig. 4. EDS element mapping profile of MT@rGO-0.1 composite (a) surface morphology and (b) carbon (red). (For interpretation of the references to color in this figure legend, the reader is referred to the web version of this article.)

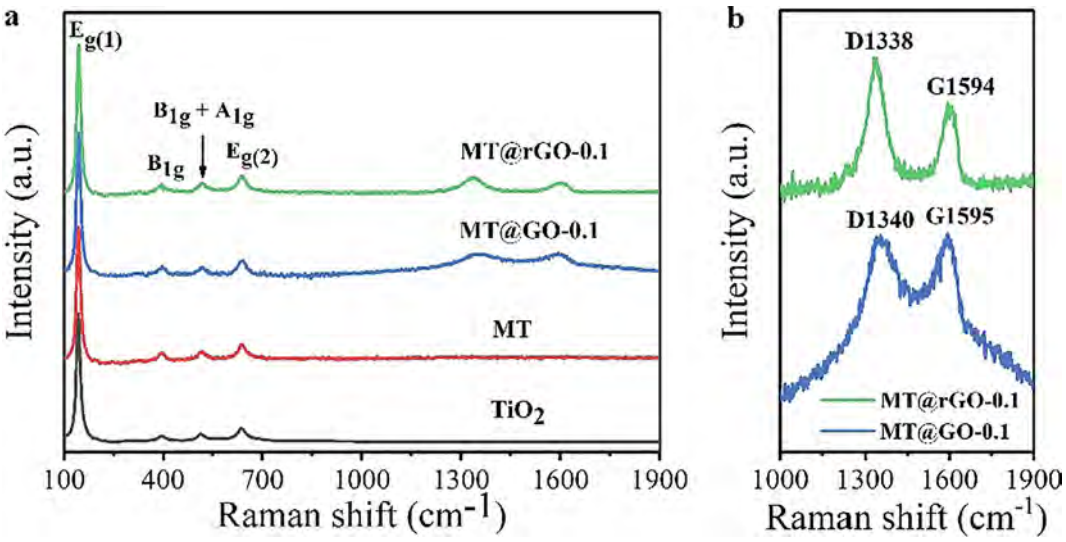

Fig. 5. (a) Raman spectra of as-prepared TiO_2 NPs, MT, MT@GO-0.1 and MT@rGO-0.1 composites; (b) locally enlarged Raman spectra of MT@GO-0.1 and MT@rGO-0.1 composites.

groups by Zn reduction. The degree of GO reduction can be quantified by the relative amount of carbon bound to oxygen, which is calculated using $(C-O)_{bond}\% = \frac{A_{C-O}+A_{C=O}}{A_{C-C}+A_{C-O}+A_{C=O}} \times 100\%$, where A_{C-C}, A_{C-O} and $A_{C=O}$ are the peak areas of graphitic carbon (C–C) and oxidized carbon (C–O, C=O), respectively [41,42]. The ratio of $(C\text{-}O)_{bond}$ in MT@GO-0.1 composite decreased from 58.8% to 50.0% of MT@rGO-0.1

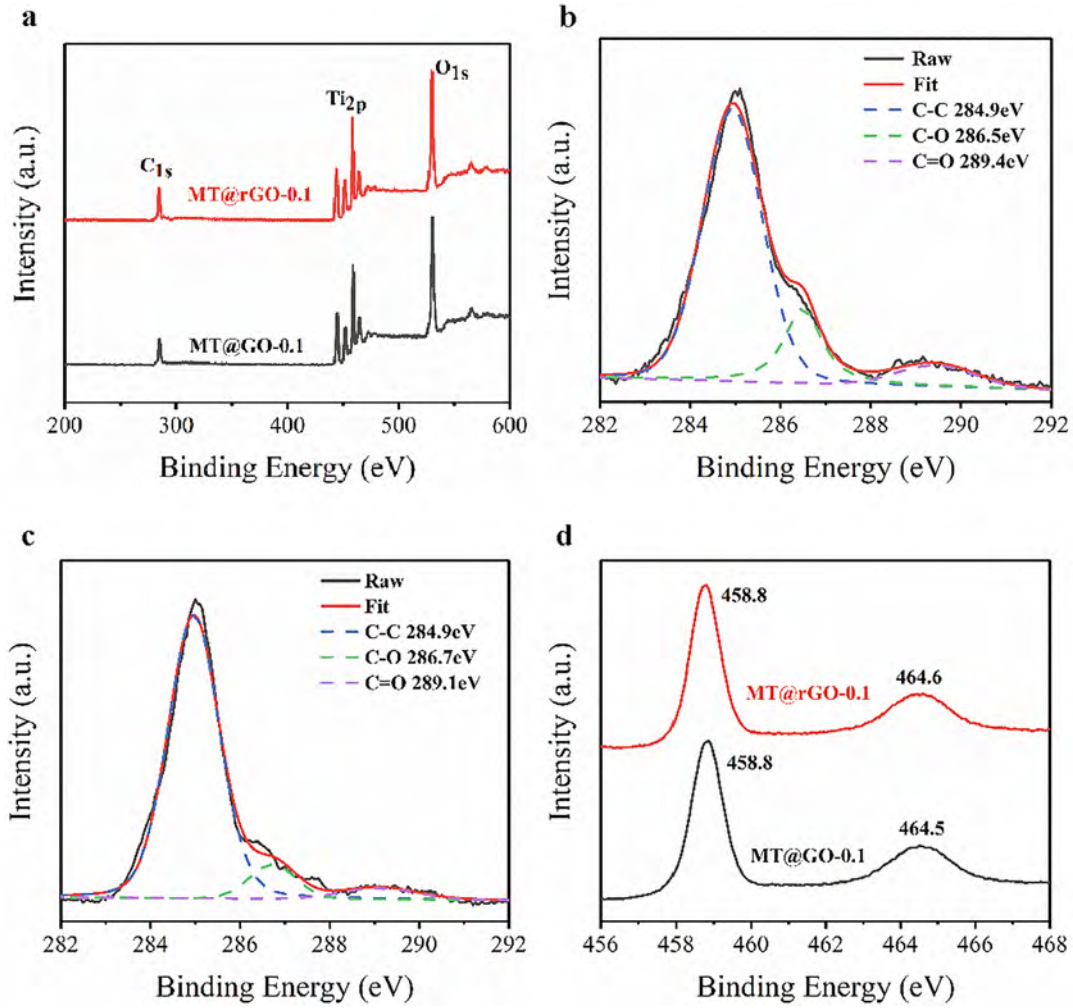

Fig. 6. (a) XPS spectra of MT@GO-0.1 and MT@rGO-0.1 composite; (b and c) the deconvoluted C 1 s spectra of MT@GO-0.1 and MT@rGO-0.1 composite; (d) Ti 2p XPS core level of MT@GO-0.1 and MT@rGO-0.1 composite.

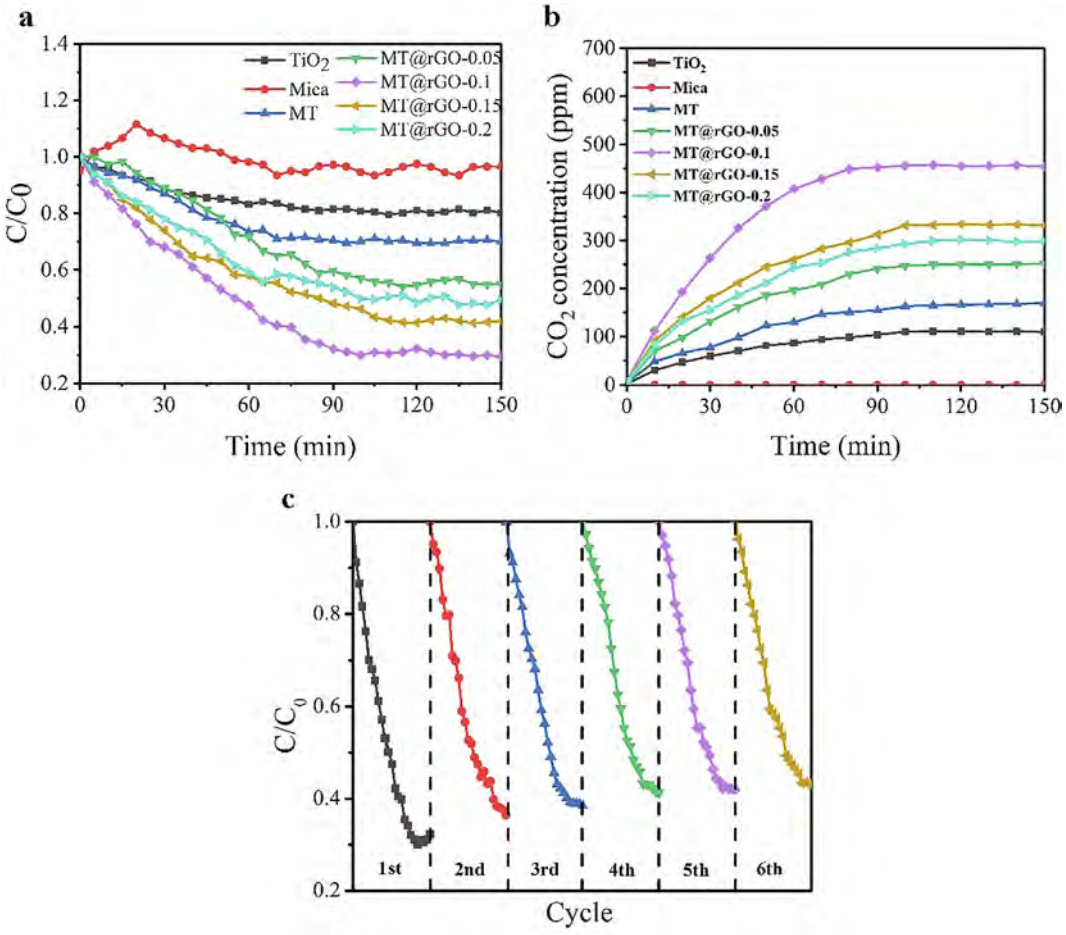

Fig. 7. (a) Photocatalytic degradation of flowing gaseous acetaldehyde (500 ppm, 8 sccm) by as-prepared TiO_2 NPs, mica, MT and MT@rGO-x (x = 0.05–0.2) composites under 400 W xenon lamp irradiation; (b) time profiles of CO_2 concentration after photodegradation; (c) cyclic experiments of acetaldehyde with MT@rGO-0.1 composite.

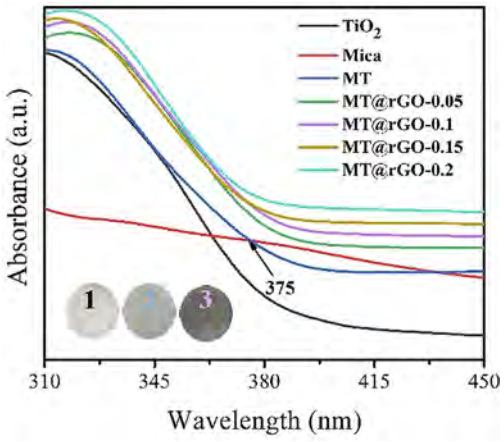

Fig. 8. UV–vis diffuse reflectance spectroscopy of TiO_2, mica, MT and MT@rGO-x (x = 0.05–0.2) composites. (Inset: optical image of TiO_2 (1), MT (2), and MT@rGO-0.1 composite (3)).

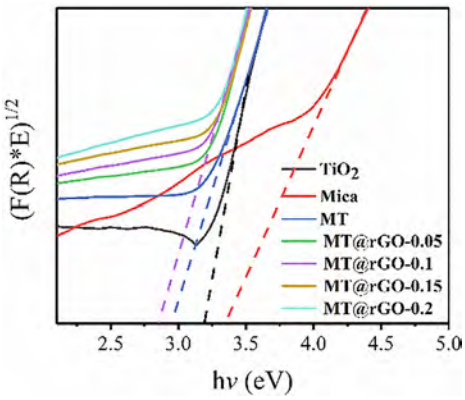

Fig. 9. The plot of the transformed Kubelka-Munk function versus the energy of light.

composite. The C/O atomic ratio increased from 0.57 to 0.65. GO was successfully confirmed to be reduced, which agrees with the Raman results [43]. In the deconvoluted Ti spectra of the composites (Fig. 6d), the peaks centered at 458.8 eV and 464.6 eV correspond to Ti $2p_{1/2}$ and Ti $2p_{3/2}$ in TiO_2. The 5.8 eV splitting between Ti $2p_{1/2}$ and Ti $2p_{3/2}$ proved the existence of Ti in the form of Ti^{4+}.

The CIE L*a*b* values of MT and MT@rGO-x (x = 0.05–0.2) composites were used to characterize the color property in Table S2. In the CIE L*a*b* system, L^*, a^* and b^* values represent the lightness ranges from 0 (pure black) to 100 (pure white), green (-)/red (+) axis, and blue (-) and yellow (+), respectively [44]. All five MT-based composites display silver color ($80.53 < L^* < 88.92$, $0.14 < a^* < 0.47$, $2.24 < b^* < 4.53$) [34]. Compared with that of MT, the L^* value of MT@rGO-x (x = 0.05–0.2) composites slightly decreases with increasing rGO content.

Table 1
The adsorption limit, bandgap and S_{BET} of as-prepared TiO_2 NPs, mica, MT and MT@rGO-0.1 composite.

Samples	Adsorption limit (nm)	Bandgap (eV)	S_{BET} (m^2/g)
as-prepared TiO_2 NPs	387	3.20	25.9
Mica	370	3.35	2.3
MT	420	2.95	13.7
MT@rGO-0.1	435	2.85	16.8

3.2. Photocatalytic activity measurement

A flowing gaseous acetaldehyde photodegradation test of as-prepared TiO_2 NPs, mica, MT and MT@rGO-x (x = 0.05–0.2) composites was carried out. As shown in Fig. 7a and b, mica (red line) could not photodegrade acetaldehyde. The as-prepared TiO_2 NPs (black line) had 20% photodegradation efficiency and 11% CO_2 mineralization efficiency, while those of MT (blue line) improved to 30% and 17%, respectively. The MT@rGO-0.1 composite (purple line) had the highest photodegradation efficiency (70%), which was 2.5 times higher than that of as-prepared TiO_2 NPs, and its CO_2 mineralization efficiency (45%) was three times higher than that of as-prepared TiO_2 NPs. Thus, it can be inferred that the photocatalytic performance of as-prepared TiO_2 NPs can be significantly improved by hybridizing with mica and rGO. A cyclic experiment of acetaldehyde photodegradation of MT@rGO-0.1 composite was used to evaluate its stability under the same experimental conditions. After five cycles, the photodegradation efficiency of MT@rGO-0.1 composite stabilized to approximately 57%. The slight decrease may be ascribed to the partly covered reactive site by intermediate compounds [45].

3.3. Photocatalytic degradation mechanism

3.3.1. Optical properties

Fig. 8 shows the absorbance of as-prepared TiO_2 NPs, mica, MT and MT@rGO-x (x = 0.05–0.2) composites ranging from 310 to 450 nm. As shown in Fig. 8, the absorbance of mica was poor and that of as-prepared TiO_2 NPs rapidly decreased. However, the absorbance of MT ranging from 350 to 375 nm was obviously higher than that of TiO_2 and mica. Considering the core–shell structure of MT, the incident light was first absorbed and transmitted by TiO_2. The transmitted incident light reached the mica and then reflected to TiO_2, which could be reabsorbed and reutilized. Thus, the light harvesting of TiO_2 could be increased. In addition, the absorbance of MT@rGO-x composite increased with increasing rGO content.

The bandgap (E_g) of the composites was obtained by applying the Kubelka-Munk method using the following equations: $A = \lg(1/R)$, $F(R) = (1-R)^2/2R$, $(h\nu F) \backsim (h\nu - E_g)$, where F is the Kubelka-Munk function, R is the reflectance, and $h\nu$ is the photo energy [46]. The E_g (Fig. 9) and adsorption limit (nm) of as-prepared TiO_2 NPs, mica, MT and MT@rGO-0.1 composite are given in Table 1 [47]. It is noted that the E_g value (2.95 eV) of MT is lower than that of TiO_2 (3.20 eV), which is ascribed to the synergistic interaction between mica and titania [48]. Compared with MT, the absorption edge of MT@rGO-0.1 composite shows a 15 nm redshift, which is assigned to the bandgap (2.85 eV). Hence, it is anticipated that the coupling of mica and rGO with TiO_2 NPs increased the light harvesting range, which eventually enhanced the photocatalytic performance [32].

3.3.2. Photogenerated electron hole separation

Electrochemical impedance spectroscopy (EIS) and the equivalent

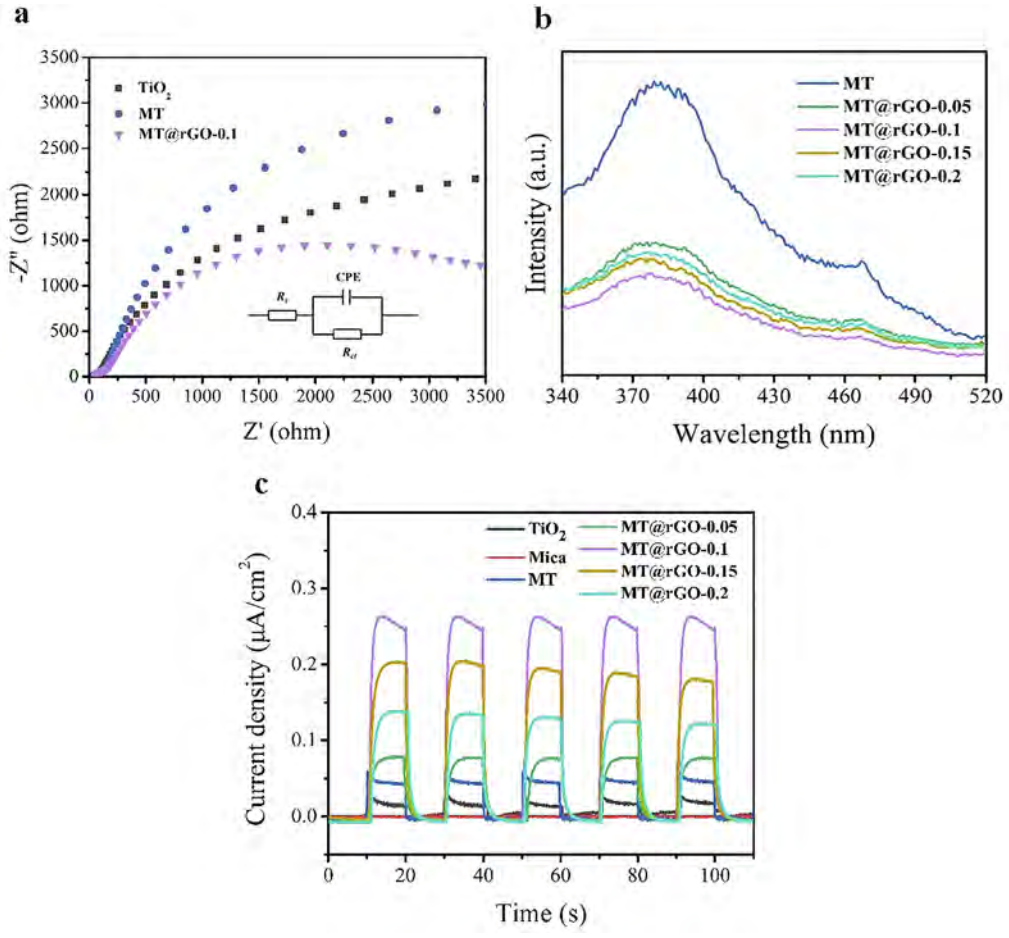

Fig. 10. (a) EIS spectra and equivalent circuit of as-prepared TiO_2 NPs, MT and MT@rGO-0.1 composite; R_s, the solution resistance; R_{ct}, the charge transfer resistance; CPE, the constant phase element; (b) PL spectra of MT and MT@rGO-x (x = 0.05–0.2) composites; (c) Photocurrent response of as-prepared TiO_2 NPs, mica, MT and MT@rGO-x (x = 0.05–0.2) composites.

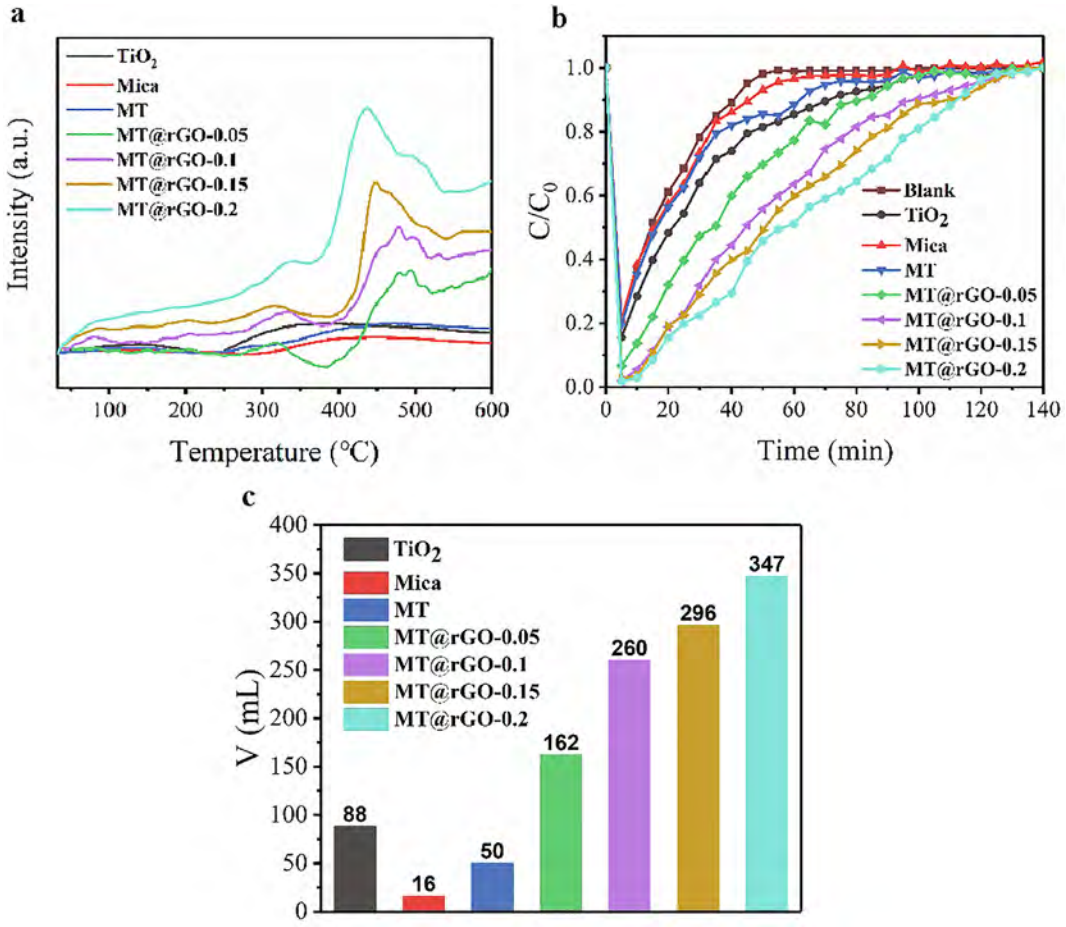

Fig. 11. (a) TPD spectra, (b) Dynamic adsorption process in 140 min and (c) The saturated adsorption amount of acetaldehyde with as-prepared TiO_2 NPs, mica, MT and MT@rGO-x (x = 0.05–0.2) composites.

circuit were employed to estimate the interfacial resistance of the composite as shown in Fig. 10a [49]. The larger arc diameter of EIS corresponds to the higher interfacial charge transfer resistance. Compared with as-prepared TiO_2 NPs, a larger arc diameter is observed in MT due to the coupling of dielectric mica. The smallest arc diameter of MT@rGO-0.1 composite represents the fastest charge transfer. The R_{ct} value of MT@rGO-0.1 composite is 6.2 kΩ, which is also smaller than that of as-prepared TiO_2 NPs (8.6 kΩ) and MT (15 kΩ). PL spectra are a useful monitor to investigate the recombination of photoinduced e^- and h^+ pairs. A higher PL intensity represents more recombination. As shown in Fig. 10b, the PL intensity of MT was higher than that of MT@rGO-x (x = 0.05–0.2) composites, which implies that MT had more recombination of photogenerated e^- and h^+ pairs, while MT@rGO-0.1 composite had the least [50]. Photocurrent measurement was used to reveal the generation and separation of e^- and h^+ pairs. The photocurrent density could be influenced by not only the utilization of incident light but also the effective transfer of charge carriers. As shown in Fig. 10c, mica had zero photocurrent density, which was in accordance with its poor photocatalytic activity. In contrast to as-prepared TiO_2 NPs, MT exhibits higher photocurrent density, implying that more photoinduced e^- and h^+ pairs were generated in MT because of its increased light harvesting. With the addition of graphene, the MT@rGO composites show higher photocurrent density than MT, among which MT@rGO-0.1 composite shows the highest photocurrent density. However, the excessive rGO could have been an electron acceptor in the composite, which may have prevented a further increase in the photocurrent density in MT@rGO-0.15 and MT@rGO-0.2. In summary, through EIS, PL and photocurrent tests, rGO was shown to effectively improve the separation of photogenerated e^- and h^+ pairs of MT.

3.3.3. The pollutant adsorption

The corresponding specific surface area (S_{BET}), temperature programmed desorption (TPD), dynamic acetaldehyde adsorption process and saturated adsorption amounts of composites were employed to estimate the relationship between the adsorption ability of gas and photocatalytic performance [51]. A larger the S_{BET} value usually indicates more absorption. As shown in Table S3, the S_{BET} value of MT (13.7 m^2/g) is five times higher than that of mica (2.3 m^2/g) and half that of as-prepared TiO_2 NPs (25.9 m^2/g). It could be assumed that micro flake MT has weak adsorption capacity. The addition of rGO increased the S_{BET} value, which is a positive development for pollutant adsorption [52].

To further explore the relationship between absorption and photocatalytic performance of the photocatalyst, TPD measurements were carried out with flowing acetaldehyde (1000 ppm, 8 sccm) at a 10 °C/min heating rate. A higher intensity of TPD represents a stronger adsorptive capacity. There were three characteristic peaks during the desorption of acetaldehyde: (1) the peak at 100–200 °C was related to weak binding for physical absorption; (2) another two peaks approximately 320 °C and 450 °C were ascribed to chemical binding adsorption of acetaldehyde as presented in Fig. 11a. Among the three peaks, the highest peak intensity of all samples was at 450 °C. Therefore, MT@rGO-x composites showed stronger chemical adsorption, whose intensity increased with increasing rGO content via the dipole–dipole interactions [53].

The dynamic adsorption and adsorptive amount of flowing acetaldehyde are presented in Fig. 11b-c. Longer adsorptive equilibrium time means greater absorption amount. The MT@rGO-x composites took over 120 min to achieve adsorptive equilibrium, longer than as-

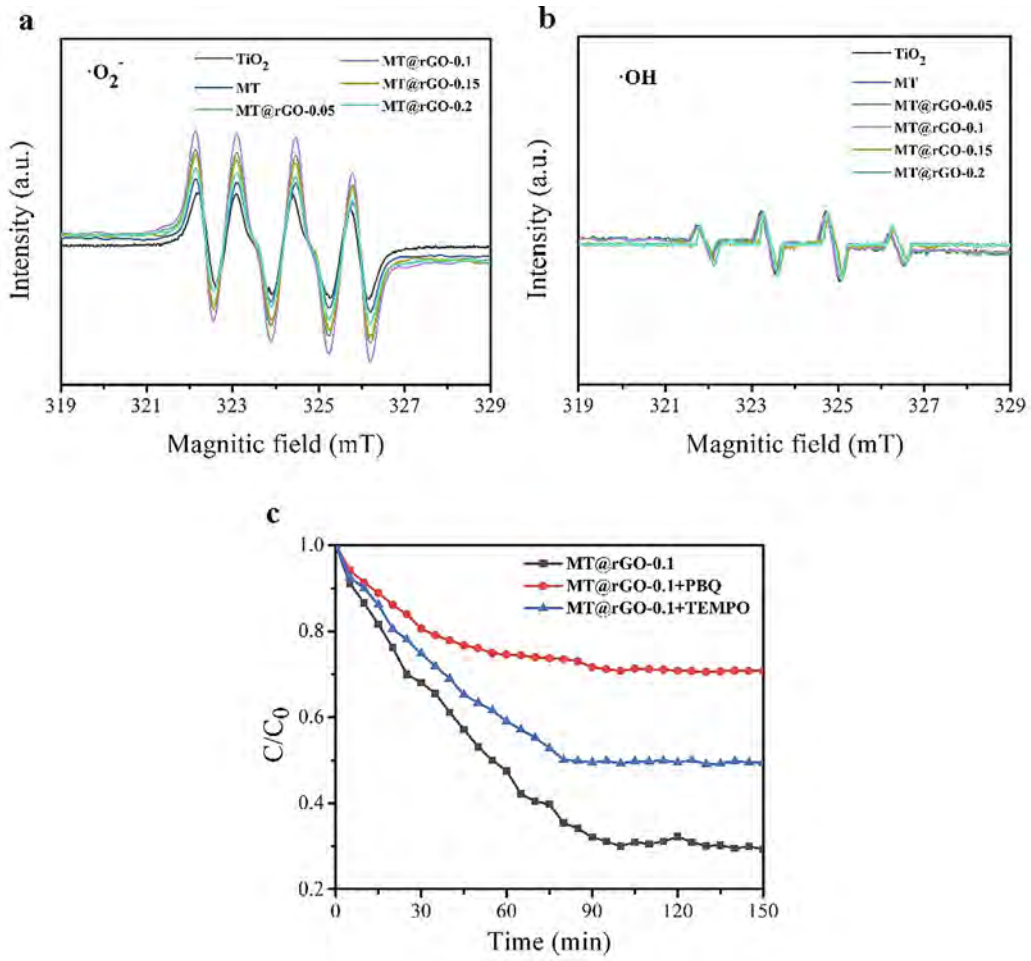

Fig. 12. (a) $\cdot O_2^-$ and (b) ·OH detection of as-prepared TiO_2 NP, MT and MT@rGO-x (x = 0.05–0.2) composites; (c) Scavenger experiments of MT@rGO-0.1 composite.

prepared TiO_2 NPs (100 min) and MT (90 min). Calculated by the area under the adsorption–desorption curve, the adsorptive amounts of acetaldehyde were 88 mL, 16 mL, 50 mL, and 162–347 mL for as-prepared TiO_2 NPs, mica, MT and MT@rGO-x composite, respectively. Thus, the addition of rGO to the ternary composite can obviously promote both the physical and chemical adsorptive performance of acetaldehyde.

3.3.4. The role of $\cdot O_2^-$ and ·OH

An electron spin resonance (ESR) test was employed to investigate the formation and yield of radicals. As shown in Fig. 12a and b, the ESR signals of as-prepared TiO_2 NPs, MT and MT@rGO-x (x = 0.05–0.2) composites with intensity ratios of 1:1:1:1 and 1:2:2:1 are classified as superoxide radicals ($\cdot O_2^-$) and hydroxyl radicals (·OH), respectively. The intensity order of $\cdot O_2^-$ is MT@rGO-0.1 > MT@rGO-0.05 > MT@rGO-0.15 > MT@rGO-0.2 > MT > as-prepared TiO_2 NPs, which suggests that the MT@rGO-0.1 composite could migrate most photoinduced electrons to absorbed O_2 to generate $\cdot O_2^-$. However, the intensity of ·OH in all samples was similar and lower than that of $\cdot O_2^-$. Therefore, it can be assumed that $\cdot O_2^-$ plays a leading role in the photodegradation of acetaldehyde of the ternary MT@rGO-x composite.

To further verify the contribution of $\cdot O_2^-$ and ·OH in the photocatalytic reaction, p-benzoquinone (PBQ, $\cdot O_2^-$ scavenger) and 2,2,6,6-tetramethyl-1-piperidinyloxy (TEMPO, ·OH scavenger) were used to quench the corresponding radicals [54,55]. The greater the decrease in photocatalytic performance, the more important role the corresponding radicals played. As seen in Fig. 12c, the photodegradation efficiency of MT@rGO-0.1 composite sharply decreased from 70% to 30% and 50% with PBQ and TEMPO, respectively, indicating that $\cdot O_2^-$ played the dominant role in the degradation.

3.4. Mechanism of enhanced photocatalytic activity

A schematic of efficient photodegradation of gaseous acetaldehyde by MT@rGO composite was proposed. As illustrated in Fig. 13, under the light excitation, the incident light that passed through rGO nanosheets to TiO_2 was harvested first. Second, the transmitted light of TiO_2 that reached mica was reflected to TiO_2 and was harvested and utilized, so more e^- and h^+ pairs were photoinduced. The electrons easily transferred to rGO owing to its low transfer resistance. $\cdot O_2^-$ was generated by the combination between electrons and absorbed O_2. The hole perching in the VB of TiO_2 transferred to the VB of mica (Fig. S1). ·OH was generated by the interaction between holes and water. Finally, gaseous acetaldehyde adsorbed on the surface of the photocatalyst could be decomposed by the two radicals. According to previous reports, we propose a possible reaction path for acetaldehyde degradation: acetaldehyde → acetic acid → formaldehyde → formic acid → CO_2 [56-59].

4. Conclusion

In summary, a ternary flake MT@rGO photocatalyst with a pearlescent effect has been designed and first applied to photodegrade flowing gaseous acetaldehyde. In this ternary system, TiO_2 NPs are

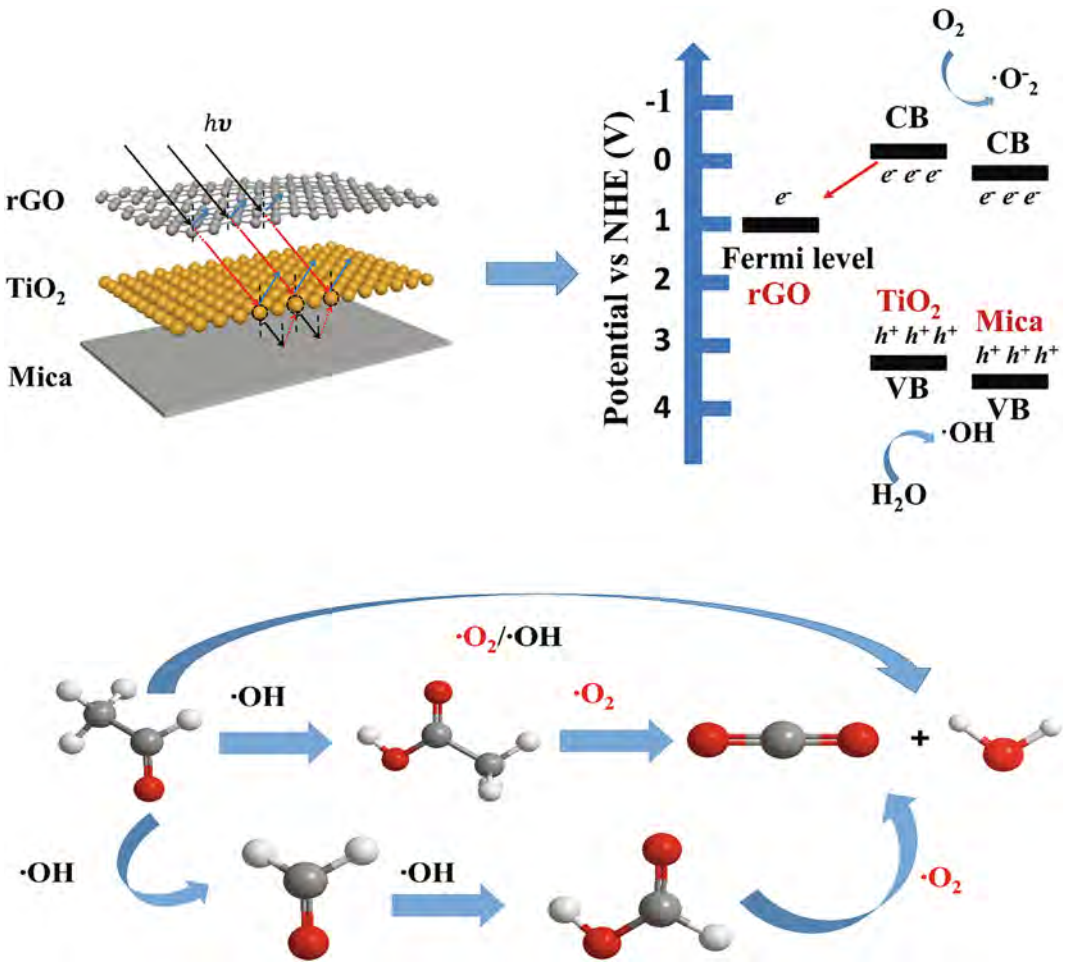

Fig. 13. Schematic of efficient photodegradation of gaseous acetaldehyde by MT@rGO composite.

homogeneously distributed on the surface of mica and intermittently coated by rGO nanosheets. MT@rGO-0.1 composite exhibits the highest acetaldehyde degradation and CO_2 mineralization efficiency, which are 2.5 times and 3 times higher than those of as-prepared TiO_2 NPs, respectively. Mica serving as a reflection core can effectively improve the light harvesting of TiO_2 NPs. rGO nanosheets employed as an electron acceptor can inhibit the recombination of photogenerated e^- and h^+ pairs. rGO also promotes the chemical and physical adsorption of acetaldehyde. These results highlight that the TiO_2-based composite coupled with a highly reflective mica core and rGO shell is favorable to the development of a next-generation photocatalyst. It is expected that MT@rGO composite with a pearlescent effect not only has high photocatalytic performance but can also be used for car paint applications.

Declaration of Competing Interest

The authors declare that they have no known competing financial interests or personal relationships that could have appeared to influence the work reported in this paper.

Acknowledgement

This work was financially supported by the National Key Research and Development Program of China (2016YFA0203000) and the National Natural Science Foundation of China (Grant No. 51702347) and the Shanghai Municipal Committee of Science and Technology Research Project (Grant No. 18142201700).

Appendix A. Supplementary data

Supplementary data to this article can be found online at https://doi.org/10.1016/j.cej.2020.125312.

References

[1] M. Amann, M. Lutz, The revision of the air quality legislation in the European Union related to ground-level ozone, J. Hazard. Mater. 78 (2000) 41–62.
[2] H.L. Chen, H.M. Lee, S.H. Chen, M.B. Chang, S.J. Yu, S.N. Li, Removal of volatile organic compounds by single-stage and two-stage plasma catalysis systems: a review of the performance enhancement mechanisms current status, and suitable applications, Environ. Sci. Technol. 43 (2009) 2216–2227.
[3] Y. Huang, S.S. Ho, K.F. Ho, S.C. Lee, J.Z. Yu, P.K. Louie, Characteristics and health impacts of VOCs and carbonyls associated with residential cooking activities in Hong Kong, J. Hazard. Mater. 186 (2011) 344–351.
[4] V. Soni, P. Singh, V. Shree, V. Goel, Effects of VOCs on Human Health, Air Pollution and Control, Springer, Singapore, 2018, pp. 119–142.
[5] X. Zhang, B. Gao, A.E. Creamer, C. Cao, Y. Li, Adsorption of VOCs onto engineered carbon materials: A review, J. Hazard Mater. 338 (2017) 102–123.
[6] S. Mudliar, B. Giri, K. Padoley, D. Satpute, R. Dixit, P. Bhatt, R. Pandey, A. Juwarkar, A. Vaidya, Bioreactors for treatment of VOCs and odours - a review, J. Environ. Manage. 91 (2010) 1039–1054.
[7] M. Stucchi, F. Galli, C.L. Bianchi, C. Pirola, D.C. Boffito, F. Biasioli, V. Capucci, Simultaneous photodegradation of VOC mixture by TiO_2 powders, Chemosphere 193 (2018) 198–206.
[8] C.H. Ao, S.C. Lee, J.Z. Yu, J.H. Xu, Photodegradation of formaldehyde by photocatalyst TiO_2: effects on the presences of NO, SO_2 and VOCs, Appl. Catal. B-Environ. 54 (2004) 41–50.
[9] Z. Shayegan, C.-S. Lee, F. Haghighat, TiO_2 photocatalyst for removal of volatile organic compounds in gas phase – A review, Chem. Eng. J. 334 (2018) 2408–2439.
[10] M.R.D. Khaki, M.S. Shafeeyan, A.A.A. Raman, W. Daud, Application of doped photocatalysts for organic pollutant degradation - A review, J. Environ. Manage. 198 (2017) 78–94.
[11] H. Park, H.-I. Kim, G.-H. Moon, W. Choi, Photoinduced charge transfer processes in

solar photocatalysis based on modified TiO_2, Energy Environ. Sci. 9 (2016) 411–433.
[12] Y. Nam, L.Q. Li, J.Y. Lee, O.V. Prezhdo'a, Strong Influence of Oxygen Vacancy Location on Charge Carrier Losses in Reduced TiO_2 Nanoparticles, J. Phys. Chem. Lett. 10 (2019) 2676–2683.
[13] A. Zaleska, Doped-TiO2 A review, Recent Pat. Eng. 2 (2008) 157–164.
[14] X. Lin, F. Rong, X. Ji, D. Fu, Carbon-doped mesoporous TiO_2 film and its photocatalytic activity, Microporous. Mesoporous. Mater. 142 (2011) 276–281.
[15] M.-H. Wu, L. Li, N. Liu, D.-J. Wang, Y.-C. Xue, L. Tang, Molybdenum disulfide (MoS_2) as a co-catalyst for photocatalytic degradation of organic contaminants: A review, Process Saf. Environ. Prot. 118 (2018) 40–58.
[16] J. Low, J. Yu, M. Jaroniec, S. Wageh, A.A. Al-Ghamdi, Heterojunction Photocatalysts, Adv. Mater. 29 (2017) 1601694.
[17] C. Adán, J. Marugán, E. Sánchez, C. Pablos, R. van Grieken, Understanding the effect of morphology on the photocatalytic activity of TiO_2 nanotube array electrodes, Electrochim. Acta 191 (2016) 521–529.
[18] X. Li, J. Yu, S. Wageh, A.A. Al-Ghamdi, J. Xie, Graphene in Photocatalysis: A Review, Small 12 (2016) 6640–6696.
[19] W. Tu, Y. Zhou, Z. Zou, Versatile Graphene-Promoting Photocatalytic Performance of Semiconductors: Basic Principles, Synthesis, Solar Energy Conversion, and Environmental Applications, Adv. Funct. Mater. 23 (2013) 4996–5008.
[20] L. Yue, R. Cheng, W. Ding, J. Shao, J. Li, J. Lyu, Composited micropores constructed by amorphous TiO_2 and graphene for degrading volatile organic compounds, Appl. Surf. Sci. 471 (2019) 1–7.
[21] W.J. Lin, X.F. Xie, X. Wang, Y. Wang, D. Segets, J. Sun, Efficient adsorption and sustainable degradation of gaseous acetaldehyde and o-xylene using rGO-TiO_2 photocatalyst, Chem Eng J 349 (2018) 708–718.
[22] X. Li, R. Shen, S. Ma, X. Chen, J. Xie, Graphene-based heterojunction photocatalysts, Appl. Surf. Sci. 430 (2018) 53–107.
[23] D.B. Nimbalkar, H.-H. Lo, P.V.R.K. Ramacharyulu, S.-C. Ke, Improved photocatalytic activity of RGO/MoS_2 nanosheets decorated on TiO_2 nanoparticles, RSC Adv. 6 (2016) 31661–31667.
[24] N. Zhang, Y. Zhang, X. Pan, M.-Q. Yang, Y.-J. Xu, Constructing Ternary CdS–Graphene–TiO_2 Hybrids on the Flatland of Graphene Oxide with Enhanced Visible-Light Photoactivity for Selective Transformation, J. Phys. Chem. C 116 (2012) 18023–18031.
[25] F. Wu, X. Li, W. Liu, S. Zhang, Highly enhanced photocatalytic degradation of methylene blue over the indirect all-solid-state Z-scheme g-C_3N_4-RGO-TiO_2 nanoheterojunctions, Appl. Surf. Sci. 405 (2017) 60–70.
[26] H.M. Yadav, J.-S. Kim, Solvothermal synthesis of anatase TiO_2-graphene oxide nanocomposites and their photocatalytic performance, J. Alloy. Compd. 688 (2016) 123–129.
[27] W. Wang, J. Yu, Q. Xiang, B. Cheng, Enhanced photocatalytic activity of hierarchical macro/mesoporous TiO_2–graphene composites for photodegradation of acetone in air, Appl. Catal. B 119–120 (2012) 109–116.
[28] B.B. Topuz, G. Gündüz, B. Mavis, Ü. Çolak, The effect of tin dioxide (SnO_2) on the anatase-rutile phase transformation of titania (TiO_2) in mica-titania pigments and their use in paint, Dyes Pigm. 90 (2011) 123–128.
[29] F.J. Maile, G. Pfaff, P. Reynders, Effect pigments - past, present and future, Prog. Org. Coat. 54 (2005) 150–163.
[30] S.S. Kim, T. Van Khai, V. Kulish, Y.H. Kim, H.G. Na, A. Katoch, M. Osada, P. Wu, H.W. Kim, Tunable Bandgap Narrowing Induced by Controlled Molecular Thickness in 2D Mica Nanosheets, Chem. Mater. 27 (2015) 4222–4228.
[31] Y. Wang, Z.W. Liu, X.Y. Lu, G.H. Lu, J. Sun, Facile synthesis of high antistatic mica-titania@graphene composite pearlescent pigment at room temperature, Dyes Pigm. 145 (2017) 436–443.
[32] H. Zhang, X. Lv, Y. Li, Y. Wang, J. Li, P25-Graphene Composite as a High Performance Photocatalyst, ACS Nano 4 (2010) 380–386.
[33] J. Qiu, C. Lai, Y. Wang, S. Li, S. Zhang, Resilient mesoporous TiO_2/graphene nanocomposite for high rate performance lithium-ion batteries, Chem. Eng. J. 256 (2014) 247–254.
[34] Y. Wang, M. Liu, Y. Liu, J. Luo, X. Lu, J. Sun, A novel mica-titania@graphene core-shell structured antistatic composite pearlescent pigment, Dyes Pigm. 136 (2017) 197–204.
[35] Y. Yu, J.C. Yu, J.G. Yu, Y.C. Kwok, Y.K. Che, J.C. Zhao, L. Ding, W.K. Ge, P.K. Wong, Enhancement of photocatalytic activity of mesoporous TiO_2 by using carbon nanotubes, Appl. Catal. a-General 289 (2005) 186–196.
[36] G.X. Wang, J. Yang, J. Park, X.L. Gou, B. Wang, H. Liu, J. Yao, Facile synthesis and characterization of graphene nanosheets, J. Phys. Chem. C 112 (2008) 8192–8195.
[37] L. Liu, S.M. Ryu, M.R. Tomasik, E. Stolyarova, N. Jung, M.S. Hybertsen, M.L. Steigerwald, L.E. Brus, G.W. Flynn, Graphene oxidation: Thickness-dependent etching and strong chemical doping, Nano. Lett. 8 (2008) 1965–1970.
[38] T. Ohsaka, F. Izumi, Y. Fujiki, Raman spectrum of anatase, TiO_2, J. Raman Spectrosc. 7 (1978) 321–324.
[39] X.G. Mei, J.Y. Ouyang, Ultrasonication-assisted ultrafast reduction of graphene oxide by zinc powder at room temperature, Carbon 49 (2011) 5389–5397.
[40] H. Liu, T. Lv, Z.F. Zhu, Template-assisted synthesis of hollow TiO_2@rGO core-shell structural nanospheres with enhanced photocatalytic activity, J. Mol. Catal. Chem. 404 (2015) 178–185.
[41] Y. Wang, J. Yu, W. Xiao, Q. Li, Microwave-assisted hydrothermal synthesis of graphene based Au–TiO_2 photocatalysts for efficient visible-light hydrogen production, J. Mater. Chem. A 2 (2014) 3847–3855.
[42] A. Iwase, Y.H. Ng, Y. Ishiguro, A. Kudo, R. Amal, Reduced graphene oxide as a solid-state electron mediator in Z-scheme photocatalytic water splitting under visible light, J. Am. Chem. Soc. 133 (2011) 11054–11057.
[43] B. Li, X.T. Zhang, X.H. Li, L. Wang, R.Y. Han, B.B. Liu, W.T. Zheng, X.L. Li, Y.C. Liu, Photo-assisted preparation and patterning of large-area reduced graphene oxide-TiO_2 conductive thin film, Chem. Commun. 46 (2010) 3499–3501.
[44] X. Wang, B. Mu, X. An, A. Wang, Insights into the relationship between the color and photocatalytic property of attapulgite/CdS nanocomposites, Appl. Surf. Sci. 439 (2018) 202–212.
[45] M.S. Kamal, S.A. Razzak, M.M. Hossain, Catalytic oxidation of volatile organic compounds (VOCs) – A review, Atmos. Environ. 140 (2016) 117–134.
[46] C.A. D'Amato, R. Giovannetti, M. Zannotti, E. Rommozzi, S. Ferraro, C. Seghetti, M. Minicucci, R. Gunnella, A. Di Cicco, Enhancement of visible-light photoactivity by polypropylene coated plasmonic Au/TiO_2 for dye degradation in water solution, Appl. Surf. Sci. 441 (2018) 575–587.
[47] S. Kaur, S. Singh, L. Singh, S.P. Lochab, Oxygen ion-induced modifications of optical properties of natural muscovite mica, Radiat Eff. Defects Solids 168 (2013) 587–593.
[48] S.X. Zuo, Z. Liu, W.J. Liu, X.Z. Li, Z.Y. Li, C. Yao, Q. Chen, Y.S. Fu, TiO_2 nanorod arrays on the conductive mica combine photoelectrochemical cathodic protection with barrier properties, J. Alloy. Compd. 776 (2019) 529–535.
[49] B.F. Xin, Z.Y. Ren, H.Y. Hu, X.Y. Zhang, C.L. Dong, K.Y. Shi, L.Q. Jing, H.G. Fu, Photocatalytic activity and interfacial carrier transfer of Ag-TiO_2 nanoparticle films, Appl. Surf. Sci. 252 (2005) 2050–2055.
[50] J. Liu, H. Bai, Y. Wang, Z. Liu, X. Zhang, D.D. Sun, Self-Assembling TiO_2 Nanorods on Large Graphene Oxide Sheets at a Two-Phase Interface and Their Anti-Recombination in Photocatalytic Applications, Adv. Funct. Mater. 20 (2010) 4175–4181.
[51] L. Huang, X. Hu, S. Yuan, H. Li, T. Yan, L. Shi, D. Zhang, Photocatalytic preparation of nanostructured MnO_2-(Co_3O_4)/TiO_2 hybrids: The formation mechanism and catalytic application in SCR deNOx reaction, Appl. Catal. B 203 (2017) 778–788.
[52] A. Giampiccolo, D.M. Tobaldi, S.G. Leonardi, B.J. Murdoch, M.P. Seabra, M.P. Ansell, G. Neri, R.J. Ball, Sol gel graphene/TiO_2 nanoparticles for the photocatalytic-assisted sensing and abatement of NO_2, Appl. Catal. B-Environ. 243 (2019) 183–194.
[53] Q.L. Zeng, X.F. Xie, X. Wang, G.H. Lu, H.W. Li, S.C. Lee, J. Sun, New insights into the synergistic effect of active radicals and adsorptive ability on the photodegradation of gaseous acetaldehyde over reduced graphene Oxide/P25 composite, J. Hazard. Mater. 380 (2019) 120814.
[54] K.L. Lv, X.J. Guo, X.F. Wu, Q. Li, W.K. Ho, M. Li, H.P. Ye, D.Y. Du, Photocatalytic selective oxidation of phenol to produce dihydroxybenzenes in a TiO_2/UV system: Hydroxyl radical versus hole, Appl. Catal. B-Environ. 199 (2016) 405–411.
[55] W.J. Li, D.Z. Li, Y.M. Lin, P.X. Wang, W. Chen, X.Z. Fu, Y. Shao, Evidence for the Active Species Involved in the Photodegradation Process of Methyl Orange on TiO_2, J. Phys. Chem. C 116 (2012) 3552–3560.
[56] X.J. Ye, D. Chen, J. Gossage, K.Y. Li, Photocatalytic oxidation of aldehydes: Byproduct identification and reaction pathway, J. Photochem. Photobiol. Chem. 183 (2006) 35–40.
[57] Q.L. Zeng, X.F. Xie, X. Wang, Y. Wang, G.H. Lu, D.Y.H. Pui, J. Sun, Enhanced photocatalytic performance of Ag@TiO_2 for the gaseous acetaldehyde photodegradation under fluorescent lamp, Chem. Eng. J. 341 (2018) 83–92.
[58] A. Fujishima, L. Sopyan, W. Mitsuru, S. Murasawa, K. Hashimoto, An efficient TiO_2 thin-film photocatalyst Photocatalytic properties in gas-phase acetaldehyde degradation, J. Photochem. Photobiol., A 98 (1996) 79–86.
[59] B. Hauchecorne, D. Terrens, S. Verbruggen, J.A. Martens, H. Van Langenhove, K. Demeestere, S. Lenaerts, Elucidating the photocatalytic degradation pathway of acetaldehyde: An FTIR in situ study under atmospheric conditions, Appl. Catal. B 106 (2011) 630–638.